RSC Advances

PAPER

View Article Online
View Journal | View Issue

Cite this: *RSC Adv.*, 2017, **7**, 8963

Development and characterization of heparin-immobilized polycaprolactone nanofibrous scaffolds for tissue engineering using gamma-irradiation

Jin-Oh Jeong,†[ac] Sung In Jeong,†[a] Jong-Seok Park,[a] Hui-Jeong Gwon,[a] Sung-Jun Ahn,[a] Heungsoo Shin,[b] Jae Young Lee[c] and Youn-Mook Lim*[a]

Polycaprolactone (PCL) has been considered a useful material for orthopedic devices and osseous implants because of its biocompatibility and bone-forming activity. However, PCL-based scaffolds have hydrophobic surfaces that reduce initial cell viability. In this study, we fabricated surface-modified PCL nanofibers for tissue engineering using radiation technology. We supplemented the hydrophilicity of the PCL nanofibers by introducing 2-aminoethyl methacrylate (AEMA) through gamma-irradiation and subsequently immobilized heparin onto the nanofibers using the EDC/NHS reaction. The SEM images show that there is almost no change in the morphology of nanofibers after radiation grafting of AEMA and heparin-immobilization onto PCL nanofibers. The surface properties of the scaffolds were characterized by ATR-FTIR, XPS, and fluorescamine staining in order to confirm the successful grafting of AEMA onto the PCL nanofibers. Immobilization of heparin was also confirmed by the amide I (1650 cm^{-1}) and amide II group (1550 cm^{-1}) from ATR-FTIR. The amounts of heparin were drastically increased on the AEMA–PCL nanofibers as revealed by TBO assay. The initial cell viability of hMSCs was significantly increased on the AEMA grafted nanofibers but grew slowly on heparin-immobilized nanofibers. The cumulative release of bone morphogenetic protein-2 (BMP-2) was slow and continuous onto the heparin-immobilized nanofibers (18.13 ± 3.87 μg mL^{-1}) compared to PCL nanofibers (20.25 ± 1.45 μg mL^{-1}). Therefore, heparin-immobilized nanofibers may be a good tool for tissue engineering applications using radiation technology.

Received 9th August 2016
Accepted 4th January 2017

DOI: 10.1039/c6ra20082f

www.rsc.org/advances

1. Introduction

For successful engineering of damaged tissues or organs, such as bone, blood vessels, and skin, the appropriate cells, growth factors, and synthetic or naturally derived scaffolds should be combined.

Recently, more focus has been given to studying bone repair due to an aging population and an increase in social activities that lead to frequent accidents. For example, damage caused by bone fractures and ligament ruptures results in increased pain in elderly individuals who have serious health problems, such as osteoporosis. Teams of tissue engineers have been actively developing three-dimensional (3D), highly porous structures to act as bioactive scaffolds for bone tissue engineering that can promote new tissue growth by assisting and speeding up the healing process.[1,2] An ideal artificial scaffold should be designed to mimic the native extracellular matrix (ECM) structure as much as possible. Scaffolds for bone regeneration need to be three-dimensional and highly porous to support uniform cell attachment and proliferation, and also need to have an interconnected and permeable pore network to promote nutrient and waste exchange. Many methods to prepare porous three-dimensional biodegradable scaffolds have been developed in bone tissue engineering, including gas forming, salt leaching/particulate leaching, overrun process, phase separation, and electrospinning.[3–7]

Electrospinning is an efficient way of producing nanofibrous structures for natural and synthetic polymers. Large pore size, thickness, and a tunable surface area to volume ratio of electrospun scaffolds are important features of tissue-engineered scaffolds that strongly enhance cellular adhesion, proliferation, and infiltration.[8,9] Typical biocompatible synthetic polymers such as poly (L-lactic acid) (PLLA), poly (glycolic acid) (PGA), poly (lactic-*co*-glycolic acid) (PLGA), and

[a]*Research Division for Industry & Environment, Advanced Radiation Technology Institute, Korea Atomic Energy Research Institute (KAERI), 29 Gumgugil, Jeongeup, 56212, Republic of Korea. E-mail: ymlim71@kaeri.re.kr; Tel: +82-63-570-3065*

[b]*Department of Bioengineering, Division of Applied Chemical and Bio Engineering, Hanyang University, Seoul 133-791, Republic of Korea*

[c]*School of Materials Science and Engineering, Gwangju Institute of Science and Technology (GIST), Gwangju 61005, Republic of Korea*

† These two authors contributed equally to this work.

polycaprolactone (PCL) have been electrospun for bone tissue engineering.[10–12]

Among the synthetic biopolymers, the FDA-approved PCL has a good mechanical strength, unique elasticity, and hardness similar to that of bone, and it degrades faster than either homopolymer. Biodegradable synthetic polymer scaffolds from electrospun PLLA nanofibers, PLGA/hydroxyapatite composites, and HA–titanium have been used for the controlled, sustained, and localized release of BMP-2.[13–15]

Bone morphogenetic protein-2 (BMP-2) is known to increase bone formation significantly and to improve the adhesion, proliferation, differentiation and mineralization of osteoblasts when incorporated within the scaffold. The advantages of using BMP-2 have also been demonstrated on nanofibrous scaffolds for bone tissue engineering. However, the release of BMP-2 was uncontrolled due to a rapid release and a short half-life of activity. To overcome these weakness, the use of heparin in creating heparin-immobilized titanium surfaces and heparin-conjugated PLGA scaffolds has been studied.[16,17]

Heparin is a sulfated glycosaminoglycan (GAG), and it has a variety of biological activities, such as the ability to induce diverse changes in the chemical structure and structural specificity of anionic functional groups. The biological activity of heparin is associated with the interaction and binding affinity to different proteins.[18] However, when introducing additional heparin, the existing heparin conjugated onto the surface of biomaterials can result in problems such as high toxicity and non-uniform surface treatment by chemical agents, UV irradiation, and thermal discharge plasma.[11,19] To overcome these problems, gamma-irradiation can be used to increase the grafting efficiency of biomaterial surfaces and also the uniformity of grafted bio-active molecules such as proteins and peptides, which can increase hydrophilicity and cell viability.[20,21]

Radiation-based modification of biomaterial surfaces should be rapidly performed in order to minimize free radical formation, as well as be carried out without chemical additives such as initiators and catalysts. In addition, it has the advantage of being able to be performed at low temperatures in gas, solid, or liquid state.[22,23] In a previous study, bacterial cellulose and PLCL film surface were grafted with acrylic acid using gamma-irradiation, and then gelatin was conjugated using the EDC/NHS reaction.[24] Based on this and other research, the use of radiation techniques seems promising for tissue engineering applications. In this study, we fabricated surface-modified PCL nanofibers using radiation techniques for bone tissue engineering. The PCL nanofibers were prepared by electrospinning, hydrophilicity was modified by grafting 2-aminoethyl methacrylate (AEMA) using gamma-irradiation, and heparin was immobilized using the EDC/NHS reaction. There is study that how to modify on the surface of PCL nanofibrous scaffolds using gamma-irradiation. Especially the irradiated PCL scaffolds can be little effected by the properties induced crosslinking and chain scission through the radiation.[25] However, this study focused on control release of BMP-2 from immobilized heparin *via* AEMA grafted PCL scaffolds using gamma-irradiation. Therefore, our strategy using radiation technology could be a promising tool for designing biomimetic scaffolds.

2. Experimental

2.1. Materials

Polycaprolactone (PCL) with a molecular weight (M_n) from 70 000 to 90 000 g mol^{-1}, 2-aminoethyl methacrylate hydrochloride (AEMA), toluidine blue O (TBO), fluorescamine, *N*-(3-dimethylaminopropyl)-*N*′-ethylcarbodiimide hydrochloride (EDC) and 2-(*N*-morpholino)ethanesulfonic acid sodium salt (MES) were obtained from Sigma-Aldrich (St. Louis, MO, USA). Tetrahydrofuran (THF) and *N*,*N*-dimethyl formamide (DMF) were purchased from Duksan reagent (Ansan, Korea) and Showa Chemical Co. (Tokyo, Japan). Dulbecco's phosphate buffered saline (DPBS), Dulbecco's modified eagle's medium (DMEM), fetal bovine serum (FBS) and streptomycin were obtained from GIBCO (Carlsbad, CA, USA). All other reagents and solvents were of analytical grade and used as received.

2.2. Preparation of AEMA-*g*-PCL nanofibrous scaffolds and gamma-irradiation

To prepare the PCL solution, PCL was dissolved in a mixture of THF and DMF (70 : 30, v/v) at room temperature (RT) to a final concentration of 13% (w/v). The PCL solution was loaded into a 12 mL plastic syringe (Henke Sass Wolf, Germany) with a blunt stainless-steel needle (20G, NanoNC, Seoul, Korea). The plastic syringe was then placed in an infusion pump (SHB366, Sckjmoter, China) and the needle connected to a high-voltage power supply (ESR-200RD, NanoNC, Korea). The solution flow rate, applied voltage, and spinning time were fixed to 1 mL h^{-1}, 11.3 kV, and 10 h, respectively. The distance between the needle and aluminum foil-wrapped rotating drum collector was fixed 15 cm. To evaporate the solvent, the PCL nanofibrous scaffolds were dried at 40 °C overnight in vacuum oven.[26] After fabrication, the samples were placed in AEMA/methanol solutions with AEMA concentrations of 1, 5 and 7% (w/v) in 10 mL glass vial. The AEMA was grafted onto PCL nanofibrous scaffolds by ^{60}Co gamma-irradiation at 25 kGy and a dose rate of 10 kGy h^{-1} at RT. All samples were washed with distilled water (DW) for 48 h at RT to remove the unreacted monomers and homopolymers. After washing, AEMA-grafted PCL nanofibers (AEP) were freeze-dried for 48 h.

2.3. Immobilization of heparin onto AEMA–PCL nanofibers using EDC/NHS reaction

To immobilize heparin onto AEMA–PCL nanofibers (H-AEP), the samples were immersed in 0.1 M MES buffer solution (pH 5.07, 5 mg mL^{-1}) for 1 h, and after that it was immersed in EDC/NHS (3 mg mL^{-1}) and heparin (2 mg mL^{-1}) dissolved in 0.1 M MES buffer solution for 12 h at RT. The samples were washed with DW to remove the unreacted monomers and homopolymers for 48 h. After washing, the H-AEP was freeze-dried for 48 h.

2.4. Characterization of nanofibers

2.4.1. Scanning electron microscopy. The morphologies of all samples were investigated using scanning electron microscopy (SEM, JSM-6390, JEOL, Japan) with an electron-beam of 10 kV and working distance of 8.1 mm. To observe the high-resolution images of the AEP and unmodified PCL nanofibers, the samples were covered with a layer of gold for 60 seconds by sputter coating.

2.4.2. Attenuated total reflection Fourier transform infrared spectroscopy. Infrared spectra of all samples were recorded using Bruker TEMSOR 37 (Bruker AXS. Inc., Germany) equipped with ATR mode over the range of 500–4000 cm^{-1} and a resolution of 4 cm^{-1} averaged over 64 scans.

2.4.3. X-ray photoelectron spectroscopy. Analysis of AEP was carried out by X-ray photoelectron spectroscopy (XPS, Theta Probe AR-XPS System, Thermo Fisher Scientific, UK) fitted with an Al Kα source (soft X-ray source at 1486.6 eV, which is monochromated). The anode was operated at 150 W (15 kV). The binding energy shifts due to surface charging were corrected using the C1s level at 284.6 eV, N1s level at 400 eV, and O1s level at 532.3 eV as an internal standard.

2.4.4. Fluorescamine staining. Levels of free primary amino groups conjugated onto AEP was determined using fluorescamine staining. Each sample was soaked in 350 μL of borate buffer (0.2 M boric acid, pH 9.2), and 150 μL of 0.01% fluorescamine in acetone. The samples were vortex mixed for 1 min, and then rapidly placed on a glass slide. The fluorescence was visualized and photographed using a Leica DM1400B (Leica Microsystems GmbH, Wetzlar, Germany) at λ_{ex} 392 nm and λ_{em} 480 nm.[27]

2.4.5. Mechanical properties. The AEP and PCL nanofibers were evaluated for their mechanical properties by using a Universal Testing Machine (Instron 5569, Instron, USA) with 5 kN load cell and crosshead speed of 10 mm min^{-1}. The samples were cut into 5 mm width × 30 mm length.

2.4.6. Toluidine blue O (TBO) assay. The amounts of H-AEP were quantified *via* TBO assay. Each sample was immersed in 500 μL of TBO solution (0.1 M HCl, 20 mg NaCl, and 4 mg toluidine blue O chloride) for 4 h at room temperature. The samples were washed with DW to remove the unreacted TBO solution for 24 h. After washing, H-AEP was dissolved in a mixture of 0.1 M NaOH and ethanol (1 : 4, v/v) until complete decolorization occured. The TBO was quantified by measuring the absorbance of each well at 530 nm using microplate reader (Powerwave XS, Biotek, VT, USA).

Table 1 Characteristic of heparin immobilized AEMA grafted PCL nanofibrous scaffolds

Sample	Concentration of AEMA (wt%)	Immobilization of heparin
PCL	—	—
1AEP	1	—
5AEP	5	—
7AEP	7	—
H-1AEP	1	O
H-5AEP	5	O
H-7AEP	7	O

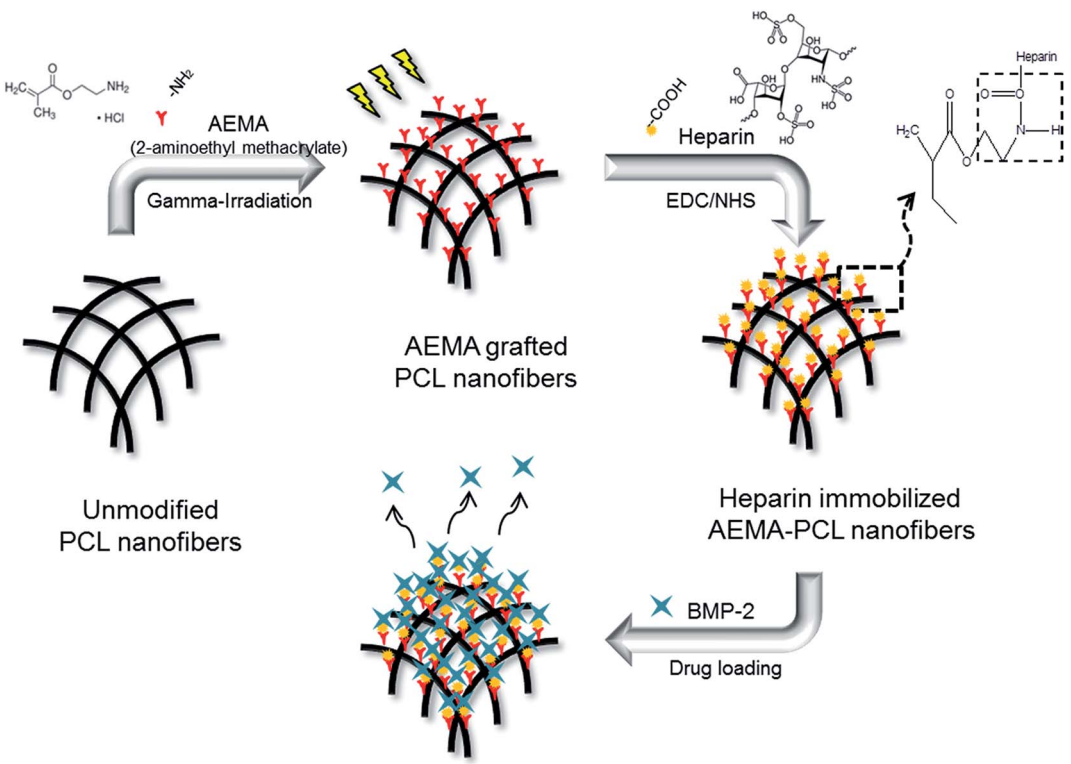

Fig. 1 Schematic diagram for the preparation of heparin-immobilized AEMA–PCL nanofibers by using gamma-irradiation.

2.5. Characterization of *in vitro* culture of hMSCs on the nanofibers

2.5.1. Human mesenchymal stem cells (hMSCs) culture. The hMSCs (CC-2519, Lonza Group Ltd., Basel, Switzerland) were seeded on the nanofibers (diameter of 10 mm, $n = 5$) at a density of 2×10^4 cells per cm^2 and then were incubated at 37 °C with 5% CO_2 atmosphere. The media was changed every two days.

2.5.2. Scanning electron microscopy. On day 1 of cell culture, the morphology of the cells on the nanofibers was investigated using SEM (JSM-6390, JEOL, Japan). The cells on the nanofiber constructs were fixed with 3.7% paraformaldehyde for 15 min at RT and then dehydrated by subjecting them to increasing concentrations of ethanol (60, 70, 80, 90, 95, and 100%). The nanofibers were covered with a layer of gold for 60 seconds by sputter coating with an electron-beam of 15 kV at a working distance of 10 mm.

2.5.3. Fluorescence staining. To observe the adherent morphology of hMSCs on the nanofibers, F-actin staining and nuclear staining was performed. After 1 day, the cells were fixed with 3.7% paraformaldehyde for 15 min at RT, then permeabilized with cytoskeletal buffer solution (10.3 g sucrose, 0.292 g NaCl, 0.06 g MgCl, 0.476 g HEPES buffer, and 0.5 mL Triton X-100 in 100 mL water, pH 7.2) for 10 min at 4 °C and blocked with 5% FBS in PBS for 1 h at 37 °C. The samples were incubated for 1 h at 37 °C in rhodamine-phalloidin (1 : 100, Molecular probes, Eugene, OR) and Hoechst 33258 (1 : 1000, Molecular probes, Eugene, OR). After washing with PBS, the samples were mounted on glass slides with mounting buffer (Vector Laboratory, UK). Immunofluorescent images were acquired using fluorescence microscope (TE2000, Nikon, Japan).

2.5.4. Cell counting kit-8 assay. On days 1, 4, and 7 of cell culture, the proliferation of the cells on the nanofibers was confirmed using CCK-8 assay. CCK-8 solution was added to nanofibers to a ratio of 9 : 1, and then incubated for 2 h at 37 °C.

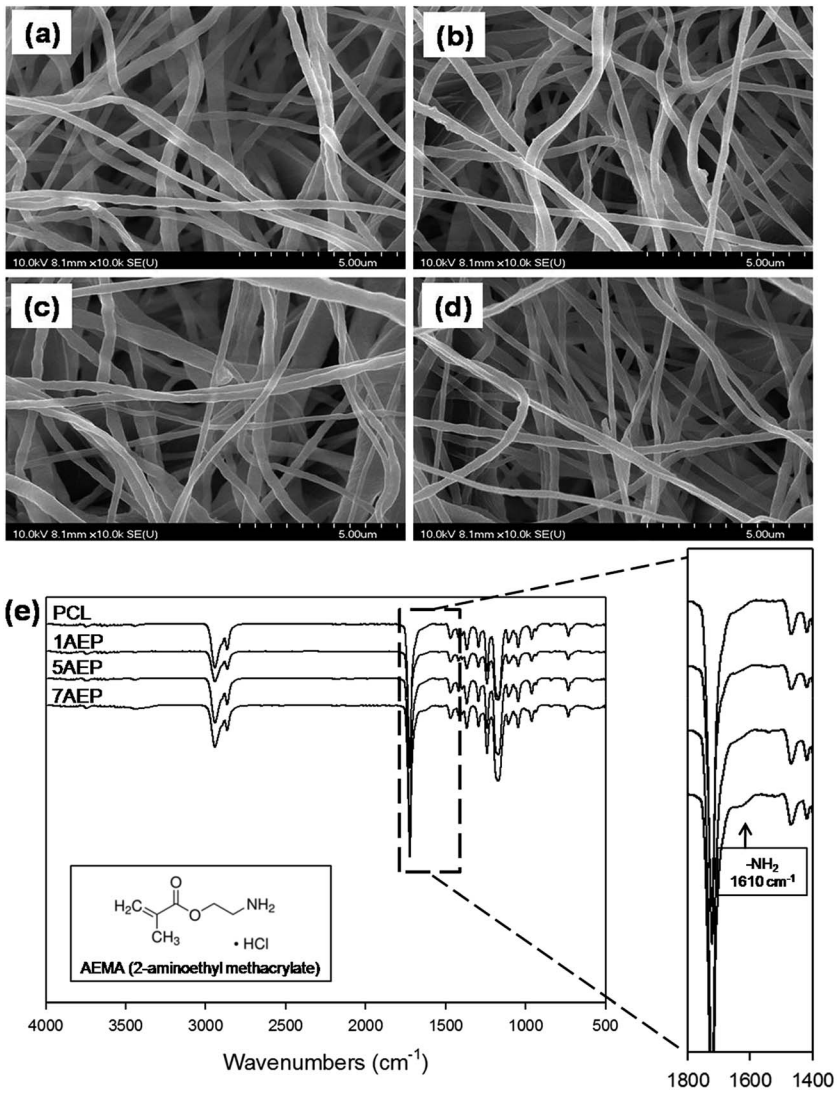

Fig. 2 SEM images of AEMA-grafted PCL nanofibers: (a) PCL, (b) 1AEP, (c) 5AEP, (d) 7AEP, and (e) ATR-FTIR spectra of PCL, 1AEP, 5AEP, and 7AEP nanofibrous scaffolds.

After the reaction, the supernatant was replaced with fresh solution and the absorbance was recorded at 450 nm.

2.6. Release test

The release of BMP-2 from PCL, 7AEP, and H-7AEP nanofibrous scaffolds was determined. All samples (diameter of 10 mm, $n = 5$) were sterilized with 70% ethanol for 12 h and then washed 3 times with PBS. The BMP-2 (25 μg mL^{-1}, Pepro Tech, Rocky Hill, NJ, USA) were incubated and completely absorbed into the nanofibers until in PBS solution for 1 h at 4 °C. The samples were incubated at 37 °C in 5 mL DMEM for 14 days and gently shaking at 100 rpm during incubating. The acquired samples through the time intervals of 1 and 12 h, and 1, 2, and 4 days were taken and replaced with PBS solution. The released BMP-2 solution into scaffolds was measured using an enzyme-linked immunosorbent assay (ELISA) development kit (Pepro Tech, Rocky Hill, NJ, USA) in a microplate reader and then the absorbance was recorded at 405 nm.[28]

2.7. Statistical analysis

All data were presented as means ± standard deviation (SD) for $n = 4$. A two-tailed unpaired Student's *t*-test (Excel, Microsoft) was used to assess statistical significance of the results ($p < 0.05$ was considered to be significant).

3. Result and discussion

3.1. Fabrication of heparin immobilized AEMA-grafted PCL nanofibers

A general schematic diagram and abbreviated samples of the H-AEP is shown in Fig. 1 and Table 1. The electrospun PCL nanofibers are characterized by a wide range of pore size distribution, high porosity, and high surface area to volume ratio, which are favorable parameters for cell attachment, growth, and proliferation. Scaffolds for tissue regeneration need to be three-dimensional and highly porous to support uniform cell attachment, proliferation, and need to have an interconnected and permeable pore network to promote nutrient and waste exchange. The design of an artificial bone substitute is to construct a scaffold for the attachment and growth of bone osteoblasts other than a permanent implant. Therefore, it can be concluded that extensive chain entanglements are necessary to produce the continuous fibers by electrospinning. Moreover, the interconnected porous structure in the scaffold would provide a chance for cytokines and growth factors to modulate bone formation. The goal of this work was threefold: (1) to prepare by deposition PCL nanofibers generated by electrospinning equipment, (2) to determine the capacity for cell adhesion and proliferation on electrospun and methacrylated PCL scaffolds, which would subsequently be radiation-grafted, and (3) to incorporate heparin into the scaffolds to provide sustained release of growth factors.[29–31] PCL nanofibers were prepared by electrospinning and then AEMA was grafted onto the PCL scaffolds to graft amino groups using gamma-irradiation. After AEMA-grafting, heparin was then immobilized by constituting amide bonds between the amino groups of AEP and the carboxylic acid groups of heparin using the EDC/NHS reaction. The BMP-2 loaded H-AEP allowed the controlled release of BMP-2 over a longer duration. There seems to be a benefit of the stably induced release of BMP-2, especially regarding the acceleration of cell adhesion and proliferation on the scaffolds.

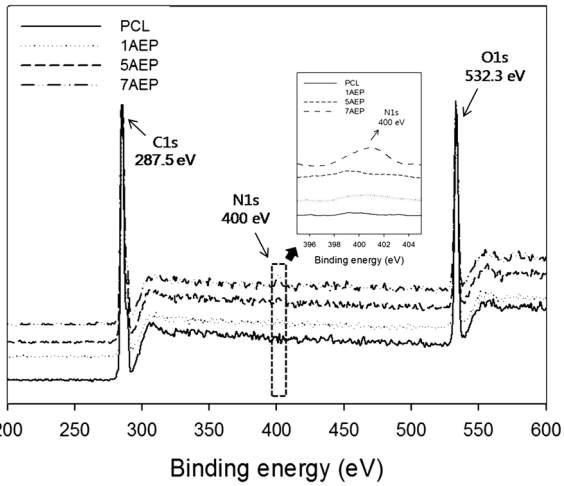

Fig. 3 XPS spectra of AEMA-grafted PCL nanofibers from 200 to 600 eV.

3.2. Characterization of AEMA-grafted PCL nanofibers

The pore size was also an important determinant for the cell migration rate inside the scaffold, as well as the time constant of biodegradation. The surface morphologies of AEP were observed by SEM with different amounts of AEMA among the

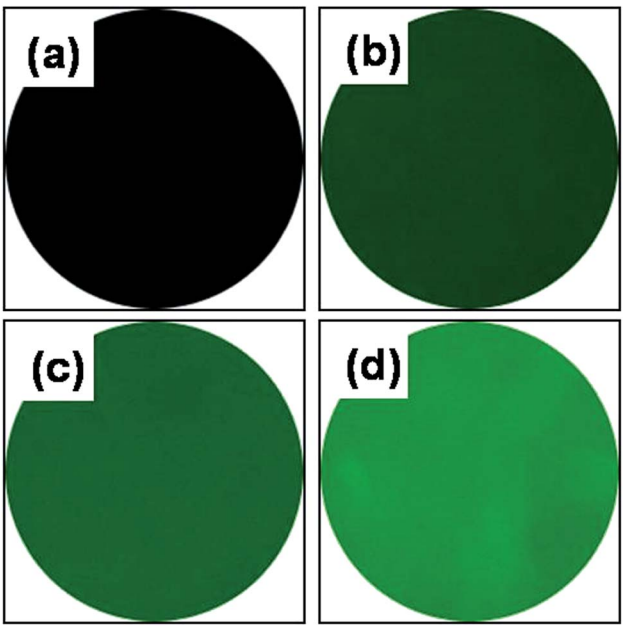

Fig. 4 Fluorescamine staining of AEMA-grafted PCL nanofibers: (a) PCL, (b) 1AEP, (c) 5AEP, and (d) 7AEP.

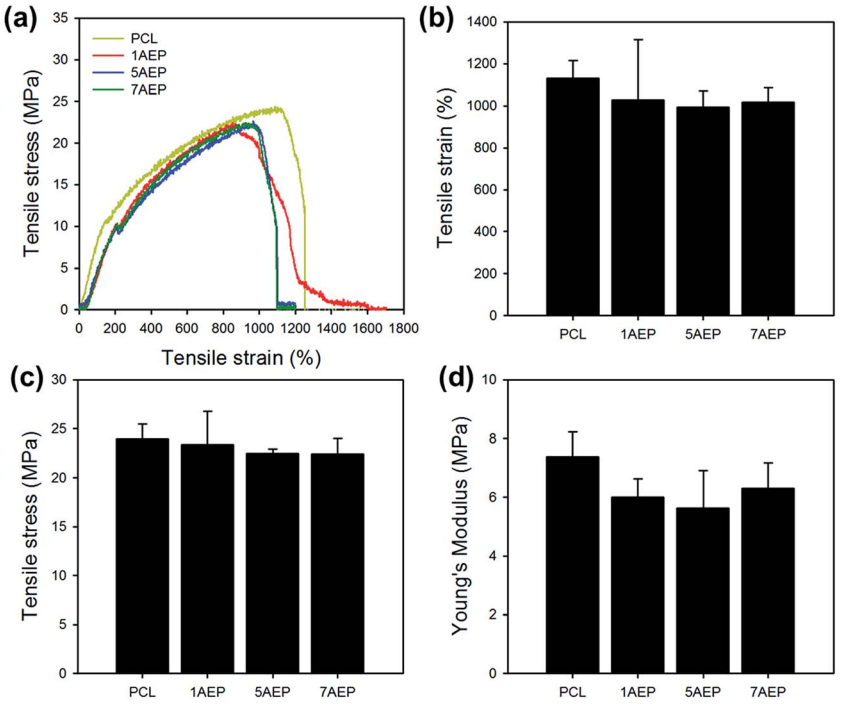

Fig. 5 Mechanical properties of AEMA-grafted PCL nanofibers: (a) tensile curve, (b) tensile strain, (c) tensile stress, and (d) Young's modulus.

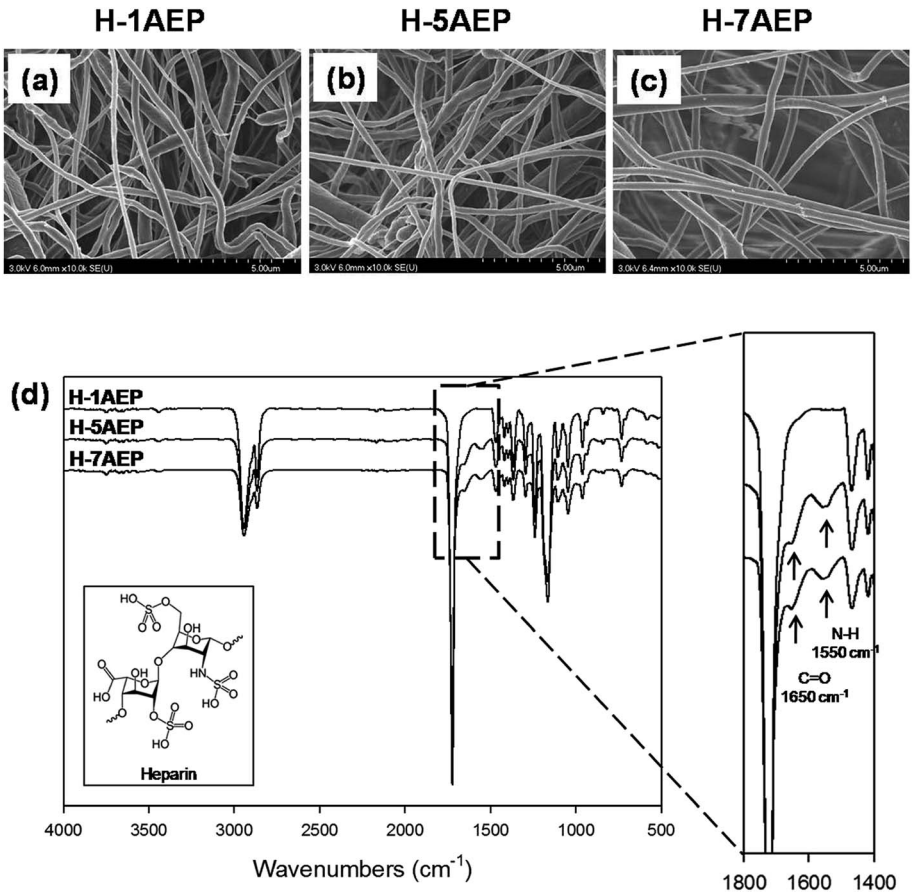

Fig. 6 (a–c) SEM images and (d) ATR-FTIR spectra of H-1AEP, H-5AEP, and H-7AEP nanofibrous scaffolds.

PCL, 1AEP, 5AEP, and 7AEP groups as shown in Fig. 2(a–d). All scaffolds appeared in the interconnected network pore configuration, characterized by its membrane-like structure. The structure was uniformly distributed, and formed an interconnected pore structure. There were no obvious morphological differences between the different AEP groups, and the diameters of the fibrous structures were similar in all the groups: PCL (226.58 ± 6.08 nm), 1AEP (220.41 ± 3.44 nm), 5AEP (222.53 ± 8.36 nm), and 7AEP (228.91 ± 3.77 nm). Therefore, there was no breakage or deformation of nanofibers after grafting AEMA using gamma-irradiation. Previously, gelatin-immobilized acrylic acid (AAc)-grafted PLCL substrates and Arg-Gly-Asp (RGD)-immobilized AAc-grafted PLLA/BCP scaffolds were also observed to have similar surface morphologies.[26,32–35] As shown in Fig. 2(e), the chemical properties of AEP were identified by ATR-FTIR, with the typical peaks of the carbonyl groups from PCL at 1700 cm^{-1}. After grafting AEMA, the amino groups of AEMA were observed at 1610 cm^{-1}. In addition, when the grafted AEMA content increased from 1 to 7 wt%, the peaks of strongest intensity were at 1610 cm^{-1} ($-NH_2$ stretching).[36,37] Thus, we found that the AEMA was successfully grafted onto the PCL. The ATR FT-IR spectra were similar to those of AEMA that include AEMA substrates.[38]

The surface composition after grafting AEMA on the PCL was observed by XPS, as shown in Fig. 3. The binding energy of PCL was located in the carbon peak (C1s peak at 287.5 eV) and oxygen peak (O1s peak at 532.3 eV), respectively. The nitrogen peak (N1s peak at 399 eV) was observed at 400 eV for the AEP.[39] While the nitrogen peak was not found in PCL, the peak intensity of nitrogen was strongest in the 7AEP group, which had a higher concentration of AEMA compared to the 1AEP and 5AEP groups. These results suggest that the radiation-induced polymerization of AEMA-grafted PCL is successful at presenting methacrylate domains at the surface of PCL nanofibers without chemical additives such as initiators and catalysts.

Qualification of AEMA grafted onto PCL nanofibrous scaffolds was confirmed with fluorescamine staining. The fluorescamine reacts with amino groups, as confirmed by use of a Leica DM1400B.[27,34] As shown in Fig. 4, pure PCL scaffolds are black in color, while the AEP uniformly exhibited green staining which increased with increasing AEMA concentrations. The 7AEP scaffolds exhibited higher intensity than 1AEP and 5AEP. This noticeable amount of grafting may result from a higher number of amino groups from AEMA induced by gamma-irradiation.

As shown in Fig. 5, the mechanical properties of PCL, 1AEP, 5AEP, and 7AEP were analyzed by UTM. The tensile stress of PCL was 23.97 ± 1.52 MPa, but for AEP was slightly decreased to 23.37 ± 1.52, 22.49 ± 0.47, and 22.46 ± 1.58 MPa according to AEMA contents of 1, 5, and 7 wt%, respectively. In addition, tensile strain and Young's modulus of AEP was also slightly decreased compared to PCL. The mechanical properties of irradiated PCL could be also decreased with increasing in irradiation dose due to significantly reduced nanofibers through both hardness and strength owing to increasing in crystallinity after irradiation.[40] Although tensile stress, tensile strain, and Young's modulus were slightly decreased, there was almost no change in mechanical properties after AEMA was grafted using gamma-irradiation within the margin of error.

3.3. Characterization of heparin immobilized AEMA-grafted PCL nanofibers

The immobilization of heparin on the AEP was activated by EDC/NHS reaction, and the heparin was immobilized by composing amide bonds between amino groups of AEP and the carboxyl groups of heparin.[24] As shown in Fig. 6(a–c), the H-AEP was identified by SEM, and the surface morphologies and fiber diameters of different H-AEP groups were similar, in keeping with the results shown in Fig. 2(a–d). In addition, the chemical properties of H-AEP were analyzed by ATR-FTIR as shown in Fig. 6(d). The amide I group (C═O stretching) and amide II group (N–H bending) were observed at 1650 cm^{-1} and 1550 cm^{-1}, respectively,[41–43] and peak intensities of amide I and amide II were increased after heparin immobilization. However, the amino group peak was decreased due to amide bond

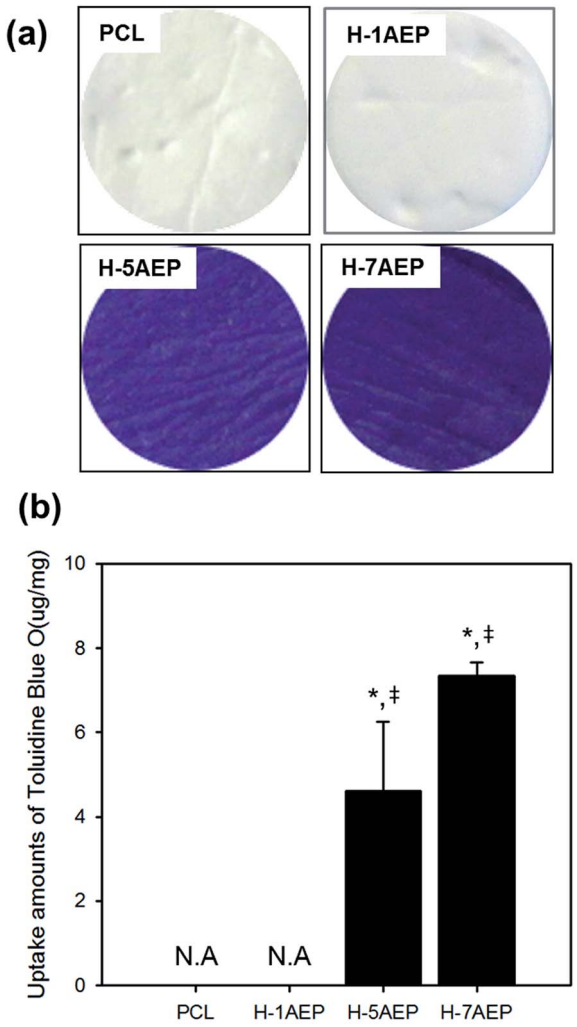

Fig. 7 (a) Staining and (b) uptake amounts of toluidine blue O (TBO) of PCL, H-1AEP, H-5AEP, and H-7AEP nanofibrous scaffolds."*" Indicates statistical significance relative to the PCL, and "‡" relative to the H-1AEP ($p < 0.05$).

formation. In addition, the intensity of the peaks increased with increasing AEMA content.

To quantify the carboxylic acid groups of heparin, a toluidine blue O (TBO) assay was used. As shown in Fig. 7(a), whereas PCL was not changed in color, the H-AEP was stained blue, with intensity also increasing according to AEMA content.[44] When the AEMA content was increased, as shown in Fig. 7(b), the amounts of TBO from the PCL and H-AEP were approximately 0, 0, 4.62 ± 1.64, and 7.35 ± 0.32 mM mg^{-1}, respectively. Therefore, heparin was successfully introduced by the EDC/NHS reaction, as confirmed by positive results from the TBO assay.

3.4. Human mesenchymal stem cell viability

The AEP allowed increased cell adhesion and proliferation of hMSCs, which highlights the importance of developing tissue engineering applications that focus on initial adhesion in order to regulate cell survival. As shown in Fig. 8(a–h), when hMSCs were cultured after 1 day, there was more adhesion on the AEP compared to PCL, as confirmed by SEM images and fluorescence photomicrographs;[39] as the AEMA content increased, the adhesion of hMSCs also increased slightly. In addition, as shown in Fig. 8(i), the cell viability of hMSCs on PCL and 7AEP was 0.96 ± 0.23 and 1.05 ± 0.14, respectively, indicating that hMSC proliferation on 7AEP was greater than on PCL, as confirmed by CCK-8 assay. This result suggests that the radiation technology used for surface modification can modify a hydrophobic surface to a hydrophilic surface without chemical additives such that cell adhesion and proliferation could be increased. However, as shown in Fig. 9(a–f), adhesion of hMSCs on the H-AEP was less spread out than on PCL, indicating that hMSCs on the H-AEP were growing more slowly as time went on. The proliferation of hMSCs is presented in Fig. 9(g); initial proliferation on the H-AEP was slow compared to the PCL. Results from the assay demonstrated significantly greater cell adhesion and proliferation on the heparin-modified materials compared to the unmodified. Also, we wanted to determine the effect of released BMP-2 from the scaffolds on hMSCs proliferation. By day seven, all scaffolds releasing BMP-2 resulted in increased cell number compared to the control (PCL), and there was increased cell number in the heparin-modified scaffold condition compared to the unmodified scaffold condition (Fig. 10).

3.5. Release test

BMP-2 was loaded for 1 h to bind with heparin and later allowed to release for 14 days. After 1 day, the cumulative release of

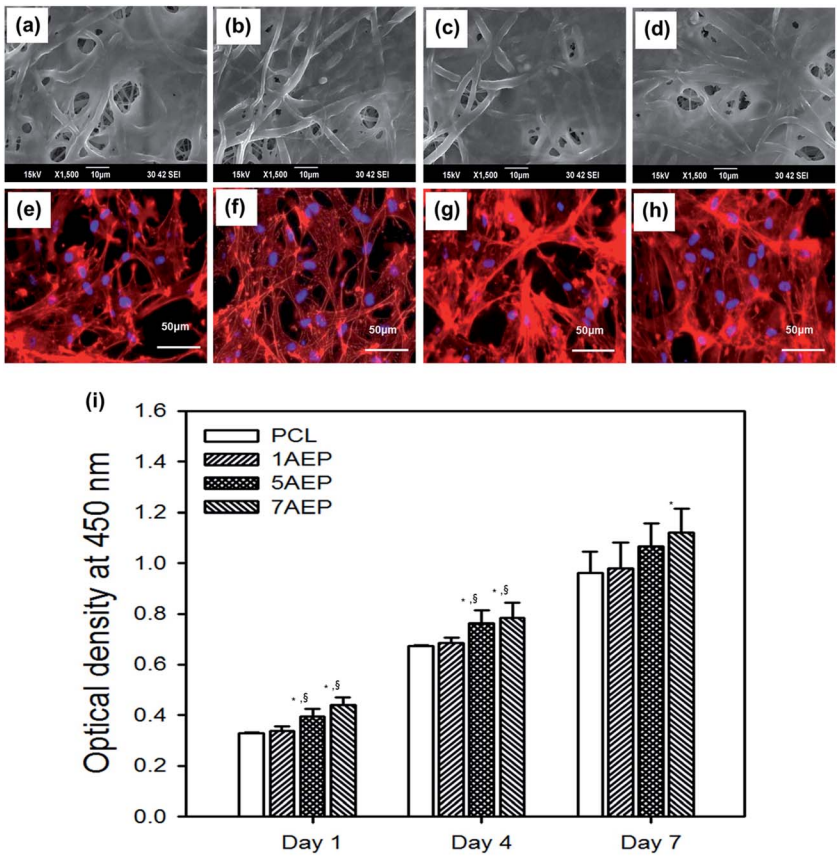

Fig. 8 SEM images and fluorescence photomicrographs of hMSCs cultured on (a, e) PCL, (b, f) 1AEP, (c, g) 5AEP, and (d, h) 7AEP nanofibrous scaffolds stained with rhodamine-phalloidin and DAPI. Scale bars represent 50 μm. (i) CCK-8 assay of hMSCs cultured on these nanofibrous scaffolds for 1, 4, and 7 days."*" Indicates statistical significance relative to the PCL, "§" relative to the 1AEP, and "‡" relative to the H-1AEP ($p < 0.05$).

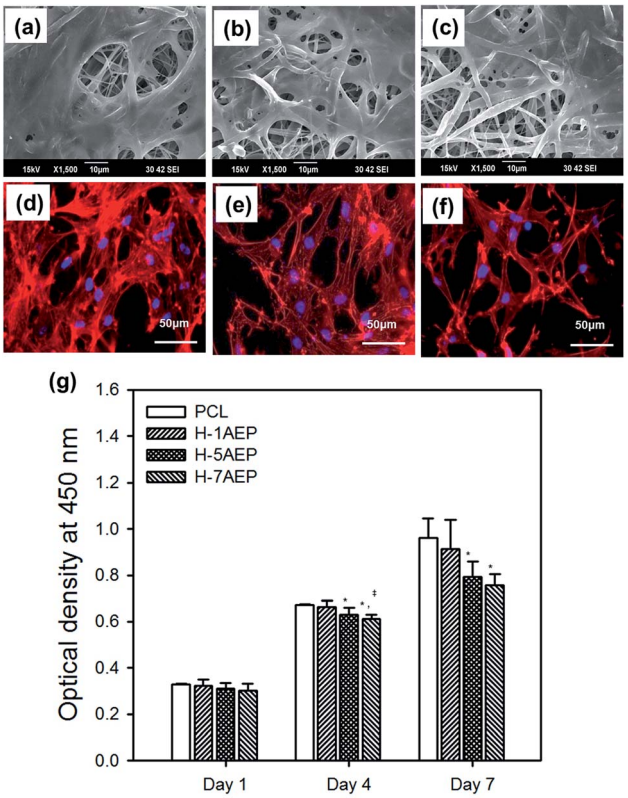

Fig. 9 SEM images and fluorescence photomicrographs of hMSCs cultured on (a, d) H-1AEP, (b, e) H-5AEP, and (c, f) H-7AEP nanofibrous scaffolds stained with rhodamine-phalloidin and DAPI. Scale bars represent 50 μm. (g) CCK-8 assay of hMSCs cultured on these nanofibrous scaffolds for 1, 4, and 7 days."*" Indicates statistical significance relative to the PCL, "§" relative to the 1AEP, and "‡" relative to the H-1AEP ($p < 0.05$).

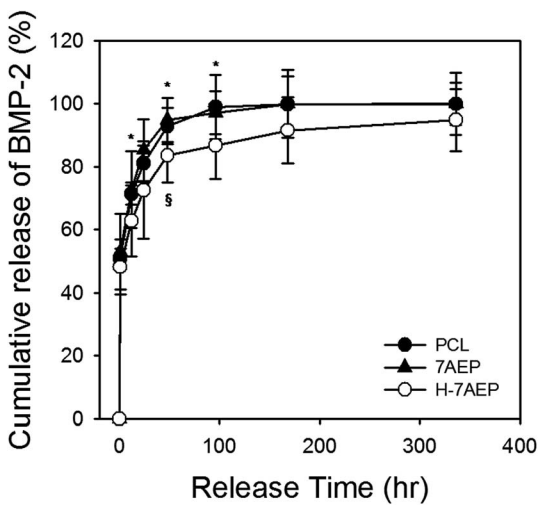

Fig. 10 Cumulative release profiles of BMP-2 from PCL, 7AEP, and H-7AEP nanofibrous scaffolds for 336 h (14 days) "*" indicates statistical significance relative to the PCL, "§" relative to the 7AEP ($p < 0.05$).

BMP-2 from PCL, 7AEP, and H-7AEP was approximately 81.02 ± 5.79, 85.30 ± 9.81, and 72.53 ± 15.48%, respectively. Therefore, BMP-2 release was decreased in H-7AEP compared to PCL, suggesting that the BMP-2 was being slowly and continuously released from the H-7AEP as time went on due to controlling effect of heparin.

4. Conclusion

In this study, to develop a biomaterial for effective regeneration in tissues, the PCL nanofibrous scaffolds were prepared by electrospinning to graft with AEMA using gamma-irradiation without chemical additives. After grafted AEMA, the heparin was then immobilized to the AEMA grafted PCL scaffolds by EDC/NHS reaction for the purpose of bone tissue engineering. The surface, chemical, and physical properties, and of these scaffolds were observed by characterization. Thus there were confirmed that AEMA and heparin were successfully and uniformly immobilized onto the PCL scaffolds through the gamma-irradiation. The modified scaffolds are successfully promoted functionalized with AEMA and heparin by radiation, and the controlled release of BMP-2 depending on immobilized heparin that was slowly released in a more biocompatible manner. Therefore, this strategy using radiation technology could be useful biomimetic scaffold applications.

Acknowledgements

This research was supported by the National Nuclear R&D program through the National Research Foundation of Korea (NRF) funded by the Ministry of Science, ICT, and Future Planning, Korea (2012M2A2A60113196).

References

1 D. H. R. Kempen, L. Lu, T. E. Hefferan, L. B. Creemers, A. Maran, K. L. Classic, W. J. A. Dhert and M. J. Yaszemski, *Biomaterials*, 2008, **29**, 3245–3252.
2 D. H. R. Kempen, L. Lu, A. Heijink, T. E. Hefferan, L. B. Creemers, A. Maran, M. J. Yaszemski and W. J. A. Dhert, *Biomaterials*, 2009, **30**, 2816–2825.
3 I. Rajzer, E. Menaszek, R. Kwiatkowski and W. Chrzanowski, *J. Mater. Sci.: Mater. Med.*, 2014, **25**, 1239–1247.
4 I. Rajzer, E. Menaszek, R. Kwiatkowski, J. A. Planell and O. Castano, *Mater. Sci. Eng., C*, 2014, **44**, 183–190.
5 Y. M. Shin, J.-S. Park, S. I. Jeong, S.-J. An, H.-J. Gwon, Y.-M. Lim, Y.-C. Nho and C.-Y. Kim, *Biotechnol. Bioprocess Eng.*, 2014, **19**, 341–349.
6 G. Wei and P. X. Ma, *Biomaterials*, 2004, **25**, 4749–4757.
7 J. Xue, M. He, H. Liu, Y. Niu, A. Crawford, P. D. Coates, D. Chen, R. Shi and L. Zhang, *Biomaterials*, 2014, **35**, 9395–9405.
8 S. I. Jeong, O. Jeon, M. D. Krebs, M. C. Hill and E. Alsberg, *Eur. Cells Mater.*, 2012, **24**, 331–343.
9 C. Zhou, Q. Shi, W. Guo, L. Terrell, A. T. Qureshi, D. J. Hayes and Q. Wu, *Eur. Cells Mater.*, 2013, **5**, 3847–3854.
10 Z. Ma, C. Gao, Y. Gong and J. Shen, *Biomaterials*, 2005, **26**, 1253–1259.
11 G. E. Park, M. A. Pattison, K. Park and T. J. Webster, *Biomaterials*, 2005, **26**, 3075–3082.

12 S. Zaiss, T. Brown, J. Reichert and A. Berner, *Materials*, 2016, **9**, 232.
13 S. E. Bae, J. Choi, Y. K. Joung, K. Park and D. K. Han, *J. Controlled Release*, 2012, **160**, 676–684.
14 T. Gao, W. Cui, Z. Wang, Y. Wang, Y. Liu, P. S. Malliappan, Y. Ito and P. Zhang, *RSC Adv.*, 2016, **6**, 20202–20210.
15 M. D. Schofer, P. P. Roessler, J. Schaefer, C. Theisen, S. Schlimme, J. T. Heverhagen, M. Voelker, R. Dersch, S. Agarwal, S. Fuchs-Winkelmann and J. g. R. J. Paletta, *PLoS One*, 2011, **6**, e25462.
16 O. Jeon, S. J. Song, S.-W. Kang, A. J. Putnam and B.-S. Kim, *Biomaterials*, 2007, **28**, 2763–2771.
17 S. E. Kim, S.-H. Song, Y. P. Yun, B.-J. Choi, I. K. Kwon, M. S. Bae, H.-J. Moon and Y.-D. Kwon, *Biomaterials*, 2011, **32**, 366–373.
18 B. Li, Z. Lin, M. Mitsi, Y. Zhang and V. Vogel, *Biomater. Sci.*, 2015, **3**, 73–84.
19 E. N. Bolbasov, M. Rybachuk, A. S. Golovkin, L. V. Antonova, E. V. Shesterikov, A. I. Malchikhina, V. A. Novikov, Y. G. Anissimov and S. I. Tverdokhlebov, *Mater. Lett.*, 2014, **132**, 281–284.
20 L. GrΦndahl, A. Chandler-Temple and M. Trau, *Biomacromolecules*, 2005, **6**, 2197–2203.
21 J. Z. Luk, J. Cooper-White, L. Rintoul, E. Taran and L. Grondahl, *J. Mater. Chem. B*, 2013, **1**, 4171–4181.
22 R. S. Benson, *Nucl. Instrum. Methods Phys. Res., Sect. B*, 2002, **191**, 752–757.
23 N. M. El-Sawy, H. A. Abd El-Rehim and A. M. Elbarbary, *Adv. Polym. Technol.*, 2011, **30**, 21–32.
24 O. Jeon, C. Powell, L. D. Solorio, M. D. Krebs and E. Alsberg, *J. Controlled Release*, 2011, **154**, 258–266.
25 E. Cottam, D. W. L. Hukins, K. Lee, C. Hewitt and M. J. Jenkins, *Med. Eng. Phys.*, 2009, **31**, 221–226.
26 S. H. Lim and H.-Q. Mao, *Adv. Drug Delivery Rev.*, 2009, **61**, 1084–1096.
27 Y.-M. Lim, S. I. Jeong, Y. M. Shin, J.-S. Park, H.-J. Gwon, Y.-C. Nho, S.-J. An, J.-B. Choi, J.-O. Jeong and J.-W. Choi, *Biotechnol. Bioprocess Eng.*, 2015, **20**, 942–947.
28 J.-B. Huh, J.-J. Yang, K.-H. Choi, J. H. Bae, J.-Y. Lee, S.-E. Kim and S.-W. Shin, *Int. J. Mol. Sci.*, 2015, **16**, 16034–16052.
29 M. C. Phipps, W. C. Clem, J. M. Grunda, G. A. Clines and S. L. Bellis, *Biomaterials*, 2012, **33**, 524–534.
30 J. R. Venugopal, S. Low, A. T. Choon, A. B. Kumar and S. Ramakrishna, *Artif. Organs*, 2008, **32**, 388–397.
31 Y. M. Shin, J.-Y. Lim, J.-S. Park, H.-J. Gwon, S. I. Jeong and Y.-M. Lim, *Biotechnol. Bioprocess Eng.*, 2014, **19**, 118–125.
32 Y. M. Shin, T. G. Kim, J.-S. Park, H.-J. Gwon, S. I. Jeong, H. Shin, K.-S. Kim, D. Kim, M.-H. Yoon and Y.-M. Lim, *J. Mater. Chem. B*, 2015, **3**, 2732–2741.
33 Y. M. Shin, S.-Y. Jo, J.-S. Park, H.-J. Gwon, S. I. Jeong and Y.-M. Lim, *Macromol. Biosci.*, 2014, **14**, 1190–1198.
34 Y. Heo, Y. M. Shin, Y. B. Lee, Y. M. Lim and H. Shin, *Colloids Surf., B*, 2015, **134**, 196–203.
35 Y. M. Shin, K.-S. Kim, Y. M. Lim, Y. C. Nho and H. Shin, *Biomacromolecules*, 2008, **9**, 1772–1781.
36 J. Kadokawa, S. Saitou and S. Shoda, *Carbohydr. Polym.*, 2005, **60**, 253–258.
37 A. R. P. Figueiredo, A. G. P. R. Figueiredo, N. H. C. S. Silva, A. Barros-Timmons, A. Almeida, A. J. D. Silvestre and C. S. R. Freire, *Carbohydr. Polym.*, 2015, **123**, 443–453.
38 O. Töpfer and G. Schmidt-Naake, *Macromol. Symp.*, 2007, **248**, 239–248.
39 H.-Y. Yu, J.-M. He, L.-Q. Liu, X.-C. He, J.-S. Gu and X.-W. Wei, *J. Membr. Sci.*, 2007, **302**, 235–242.
40 L. A. Bosworth, A. Gibb and S. Downes, *J. Polym. Sci., Part B: Polym. Phys.*, 2012, **50**, 870–876.
41 U. Edlund, S. Danmark and A.-C. Albertsson, *Biomacromolecules*, 2008, **9**, 901–905.
42 C.-H. Chang, W.-Y. Huang, C.-H. Lai, Y.-M. Hsu, Y.-H. Yao, T.-Y. Chen, J.-Y. Wu, S.-F. Peng and Y.-H. Lin, *Acta Biomater.*, 2011, **7**, 593–603.
43 X.-J. Huang, D. Guduru, Z.-K. Xu, J. Vienken and T. Groth, *Acta Biomater.*, 2010, **6**, 1099–1106.
44 J. Lee, J. J. Yoo, A. Atala and S. J. Lee, *Acta Biomater.*, 2012, **8**, 2549–2558.

